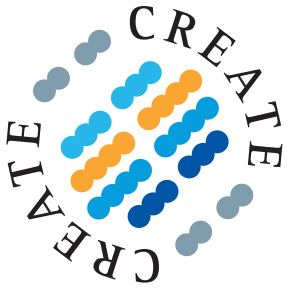

***CRITICAL RAW MATERIALS ELIMINATION BY A TOP-DOWN APPROACH TO HYDROGEN AND ELECTRICITY GENERATION***

***Grant agreement no.: 721065***

***Start date**: 01.01.2017 – **Duration**: 48 months*

***Project Coordinator**: CNRS*

# DELIVERABLE REPORT

| ***DELIVERABLE 3.5 – CRM-FREE METAL/METAL (OXY)HYDROXIDES AS HOR / HER CATALYSTS: SYNTHESIS, CHARACTERIZATION AND PERFORMANCE IN AEMFC & AEMEL*** | |
|---|---|
| Due Date | 31/12/2020 |
| Author(s) | Serhiy Cherevko, Tanja Kallio, Dario R. Dekel, Farhan S. M. Ali, Florian D. Speck , Tristan Asset, Frédéric Jaouen |
| Work Package | WP3: Catalyst synthesis and characterization |
| Work Package Leader | Tanja Kallio (AALTO) |
| Lead Beneficiary | AALTO |
| Date released by WP Leader | 27/01/2021 |
| Date released by Coordinator | 27/01/2021 |

| ***DISSEMINATION LEVEL*** | | |
|---|---|---|
| **PU** | *Public* | ***PU*** |
| **PP** | *Restricted to other programme participants (including the Commission Services)* | |
| **RE** | *Restricted to a group specified by the consortium (including the Commission Services)* | |
| **CO** | *Confidential, only for members of the consortium (including the Commission Services)* | |

| ***NATURE OF THE DELIVERABLE*** | | |
|---|---|---|
| **R** | *Report* | ***R*** |
| **P** | *Prototype* | |
| **D** | *Demonstrator* | |
| **O** | *Other* | |

## SUMMARY

| | |
|---|---|
| **Keywords** | hydrogen oxidation reaction, hydrogen evolution reaction, alkaline media, electrocatalyst, catalyst, critical raw material |
| **Full Abstract (Confidential)** | This report presents the consortium's work on PGM free catalysts for the alkaline hydrogen evolution (HER) and oxidation (HOR) reactions. As the most promising CRM-free material, Ni was in focus for both reactions. First, HOR was studied in a liquid electrolyte. Here, various alloying approaches have been considered with the intention that small amounts of Fe, Co, and Cu can potentially influence the adsorption energy of the reaction intermediates and, hence, the HOR activity. Preliminary investigation was also carried out on Ni/C & $Ni_xN$/C electrocatalysts for the HOR. Besides the activity, stability was investigated. Some alloying metals, such as Mo and Cu were ruled out due to dissolution during accelerated stress testing in ICP-MS. Another shortcoming of the Ni materials has been shown to be their low nobility, resulting in the irreversible oxidation and passivation of Ni surface at high HOR potentials. Similar results were obtained for NiMo HER catalysts that suffer severe Mo leaching during open circuit potential (OCP). On the other hand, stable Ni and NiFe Catalysts supported on CNTs showed up to 300 mV higher overpotentials than the internal target.<br>For PGM-free AEMFC presented herein, the low nobility of Ni resulted in power densities of only 56 mW $cm^{-2}$ (compared to *ca* 1.5 W $cm^{-2}$ for a PGM-free cathode paired with a high PGM content anode). For PGM-free AEMEL, the obtained activity of FeNi/CNT catalysts would result in higher electrolyzer cell voltages of ca 250-300 mV compared to an AEML with a Pt/C cathode. Therefore, the fields of PGM-free HOR and HER electrocatalysis requires significant attention to achieve PGM-free cells with high performance. |
| **Publishable Abstract (If different from above)** | |


## REVISIONS

| Version | Date | Changed by | Comments |
|---|---|---|---|
| **1.0** | 28.10.2020 | (JUL) | |
| **1.1** | 18.11.2020 | (Aalto) | |
| **1.2** | 30.11.202020 | (JUL) | |
| **1.3** | 01.12.2020 | (CNRS) | |
| **1.4** | 27.01.2021 | (CNRS) | |
| **1.5** | 31.01.2021 | (JUL) | |

# D3.5 - CRM-FREE METAL/METAL (OXY)HYDROXIDES AS HOR/HER CATALYSTS: SYNTHESIS, CHARACTERIZATION AND PERFORMANCE IN AEMFC & AEMEL

## CONTENTS

# 1 INTRODUCTION

The two-electron hydrogen reactions, namely, the hydrogen evolution reaction (HER) occurring at the electrolyzer (EL) cathode and the hydrogen oxidation reaction (HOR) at the fuel cell (FC) anode, are usually dubbed as kinetically simple reactions when compared to the oxygen reactions. The respective catalysts typically experience potentials below 0 $V_{RHE}$ (depending on their activity more or less negative) during the HER and between 0-0.4 $V_{RHE}$ during the HOR. Nevertheless, especially if alkaline media is considered, both reactions currently still rely on the utilization of noble metals for their catalysis, mainly platinum and ruthenium.

The aim in D3.5 is to identify and characterize a set of platinum group metal (PGM) free Ni-based HER/HOR catalysts towards their activity and stability in alkaline media. As up to date, no PGM free catalysts with satisfactory activity and stability exist, especially for HOR, addition of ultra-low amounts of Pt and Pd was also considered. Selected materials were to be tested in anion exchange membrane (AEM) fuel cell and electrolyzer. While the activity can be easily accessed in rotating disk electrode (RDE) measurements at the intended operating potentials, stability investigations need to consider various degradation modes ranging from dissolution during operation as well as during open-circuit potentials (OCP). When the device is switched off, and hydrogen flushed with air at the anode side, the anode's OCP equilibrates, depending on the oxygen reduction reaction (ORR) activity of the anode catalyst, but may reach up to *ca* 1 $V_{RHE}$. Furthermore, next to dissolution, other factors such as thermodynamic transitions of a material need to be considered. Therefore, stability test need to be carried out in a broad potential range over prolonged periods of time in accelerated stress tests (AST).

Test protocols for the electrochemical activity and durability measurements as well as pass/fail criteria for catalyst intended for each reaction were defined in WP2 (Technical Specifications, Cost Analysis & Life Cycle) of CREATE, and reported in Deliverable 2.1. In the following, the material performance is reflected against these criteria. Furthermore, the catalysts stability was scrutinized in prolonged electrochemical and chemical degradation test and quantified with state of the art on-line techniques such as inductively coupled plasma mass spectrometry (ICP-MS).

# 2 HOR CATALYSTS

## 2.1 $Ni_3M$ ALLOY NANOPARTICLES

### 2.1.1 SYNTHESIS OF HOR CATALYSTS (TECHNION)

Nanoparticles of the stoichiometry $Ni_3M$ (M = Mo, Cu, Co, Fe), as well as pure Ni nanoparticles, were synthesized on carbon black by a borohydride reduction reaction of the metal precursors at low temperatures.[1] In short, carbon (100 mg, VXCMAX22, CABOT) was suspended in isopropanol (15 mL, 99.9%, Sigma Aldrich) and an aqueous metal solution precursors, using an ultrasonic bath. Precursors included $NiCl_2{\times}6H_2O$ (1.7 mmol $L^{-1}$, 99.3%, Alfa Aesar), $MoNa_2O_4{\times}6H_2O$ (0.57 mmol $L^{-1}$, Alfa Aesar), $CuSO_4{\times}5H_2O$ (0.57 mmol $L^{-1}$, Emsure®, Merck), $CoCl_2{\times}6H_2O$ (0.57 mmol $L^{-1}$, 99.99%, Alfa Aesar), $FeCl_2{\times}4H_2O$ (0.57 mmol $L^{-1}$, 99.95%, Sigma Aldrich) dissolved in water (15 mL). The precursor solution was subsequently deaerated and cooled to 0 °C, before a 0 °C cold solution of $NaBH_4$ (3.4 mmol, 99.99%, Sigma Aldrich) in KOH (25 mL, 0.1 mol/L, Bio-Lab Ltd.) was slowly added while stirring. The precipitate was centrifuged and washed with water five times. The final catalyst was dried at 80 – 90 °C for 24 h.

### 2.1.2 ELECTROCHEMICAL ACTIVITY AND STABILITY (JUELICH)

Catalyst samples were drop cast on glassy carbon (GC) electrodes from an ink. In short, 10 mg of the catalyst was dispersed in 2 mL of isopropanol/water (3/1). Nafion was added to achieve an ionomer mass 40% of the mass of the catalyst. Potential dependent dissolution was measured online using a NexION 350X ICP-MS (Perkin Elmer) connected to a custom build electrochemical scanning flow cell (SFC). Here the catalyst was contacted with a 2 mm wide opening of a V-channel polycarbonate SFC. The channels were connected to a counter (graphite) and reference (Ag/AgCl) electrodes. The potential was controlled using a Reference 600 (Gamry) Potentiostat. A Peristaltic pump facilitated the electrolyte (0.05 M KOH) transport from the SFC to the ICPMS for online dissolution detection. Accelerated stress tests were carried out in a commercial three-electrode glass container (Pine) in 0.05 M KOH.
To simulate long term exposure to high pH, temperatures, and potentials, the catalyst (50 mg) was placed in 50 mL 1 M KOH and heated under ambient atmosphere at 60 °C for 30 days. Afterwards it was separated via centrifugation again, and both the catalyst as well as the electrolyte underwent physical analysis by XRD, XPS, TEM and ICP-MS.

### 2.1.3 ELECTROCHEMICAL ACTIVITY AND STABILITY RESULTS

The electrochemical HOR activity of these samples is reported by Technion.[2] Within the CREATE project, the stability of 4 different dopant in a $Ni_3M$ system was investigated using online ICP-MS (**Figure 1**). We differentiate their stability in 3 categories: corrosion, transient-dissolution, and immunity. Thermodynamically, Mo cannot form a stable phase in alkaline environments above E = -0.2 $V_{RHE}$ and corrodes drastically upon contact leaving a porous Ni rich surface. As a dopant Cu is stable at low potentials, but when oxidizing it at E > 0.4 $V_{RHE}$, it undergoes transient dissolution initiate by surface rearrangement. The three metals Ni, Co and Fe are immune during the entire protocol and their dissolution cannot be detected by ICPMS. Therefore, we focus on $Ni_3Fe$ as a stable HOR catalyst to investigate further degradation pathways.

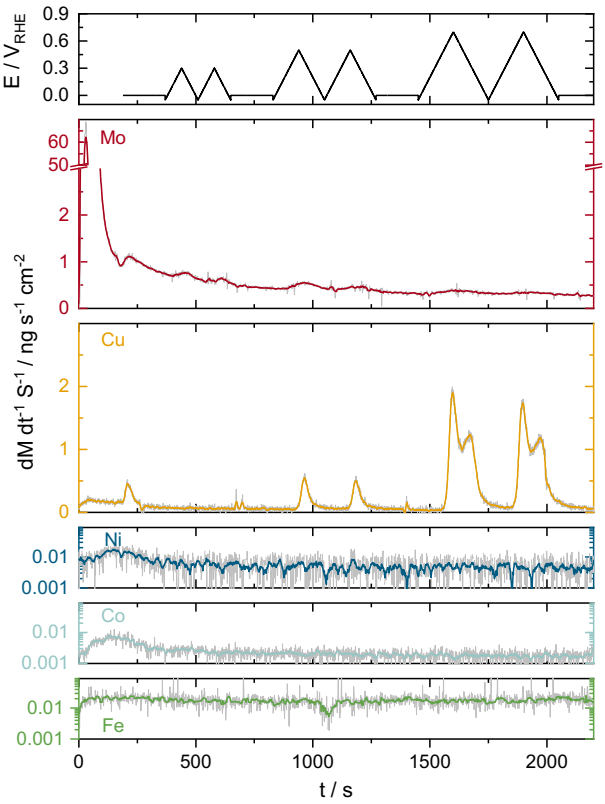


*Figure 1. Top panel shows the applied potential over time, while the bottom coloured panel show the dissolution rate of the individual metals during that same potential protocol.*

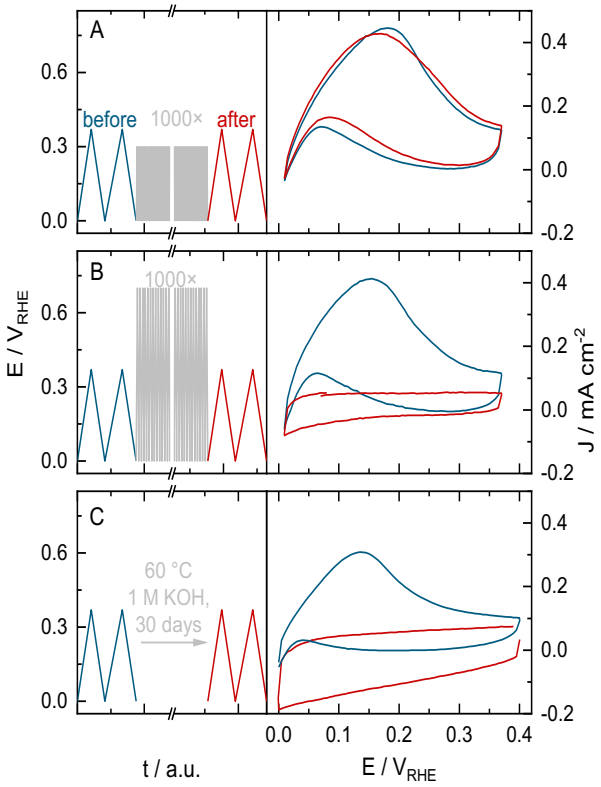


*Figure 2. Activity of $Ni_3Fe$ before and after various ASTs. (A) 1000 CVs from 0 – 0.3 $V_{RHE}$ (B) 1000 CVs from 0 – 0.7 $V_{RHE}$ (C) chemical degradation at 60 °C in 1 M KOH.*

The Thermodynamic potential of Ni oxidation is E = 0.11 $V_{RHE}$ with an expected kinetic overpotential. The metallic Ni catalyst should passivate, which is observed in the CV of **Figure 2A**. The HOR current passes its maximum at roughly 0.18 $V_{RHE}$. Afterward, instead of a diffusion-limited current behaviour, we observe fast passivation of the Ni, which is still reversible after 1000 AST cycles to 0.3 $V_{RHE}$. However, at higher AST potentials of 0.7 $V_{RHE}$, the catalyst is fully passivated (**Figure 2B**). The same irreversible passivation of HOR activity was observed in a chemical aging procedure (**Figure 2C**), where the catalyst was left for 30 days in a 1 M KOH bath at 60 °C to imitate long term exposure to hot alkaline environments. To understand the process behind this passivation, even though no dissolution was detected previously, the aged catalyst was subjected to in-depth physical analysis summarized in **Figure 3**. All techniques point towards a transformation of the initial nanoparticles into a crystalline $Ni(OH)_x$ structure. TEM images (**Figure 3A**) show a morphology change from nanoparticles, to a plate-like structure which seems to be crystalline. As confirmed by XRD (**Figure 3B**), the nanoparticles are crystalline with a broad refraction close to the literature values of Ni. Small deviations from pure Ni were attributed to the slightly larger Fe atoms in the lattice, which leads to lattice strain and a shift in the Bragg refractions.[1] After chemical aging, crystalline refractions are attributed to α– and β–$Ni(OH)_2$, while the previously alloyed iron is now a separated crystallite in the $Fe_3O_4$ phase. Here, analysis using the Scherrer equation crystallite sizes are estimated to be 10 nm ($Ni(OH)_2$ and 34 nm ($Fe_3O_4$). XPS (**Figure 3C**) also shows that Ni nanoparticles' initial surface is oxidized, which has been reported for this type of synthesis approach.[2] However, the fact that there is still 20% of metallic Ni shows that the core is metallic. Last, the degree of catalyst oxidation was tracked using $H_2$-TPR (**Figure 3D**). The TPR $H_2$ consumption as a function of temperature shows two peaks. Region I is assigned to bulk nickel oxide species, while region II can vary depending on the support material and the associated interactions.[3-5] Therefore, the first peak in the pristine catalyst corresponds to surface NiO

reduction, while the degraded sample consumes $H_2$ during $Ni(OH)_2$ reduction. Most importantly, the overall consumed $H_2$ shows full oxidation after aging (13.9 mmol $g^{-1}$), while the pristine catalyst only consumed 2.6 mmol $g^{-1}$. Therefore, the physical analysis conclusively shows full reorganization of the $Ni_3Fe$ catalyst during aging. Morphological and physical changes lead to the passivation of HOR.[1,6]

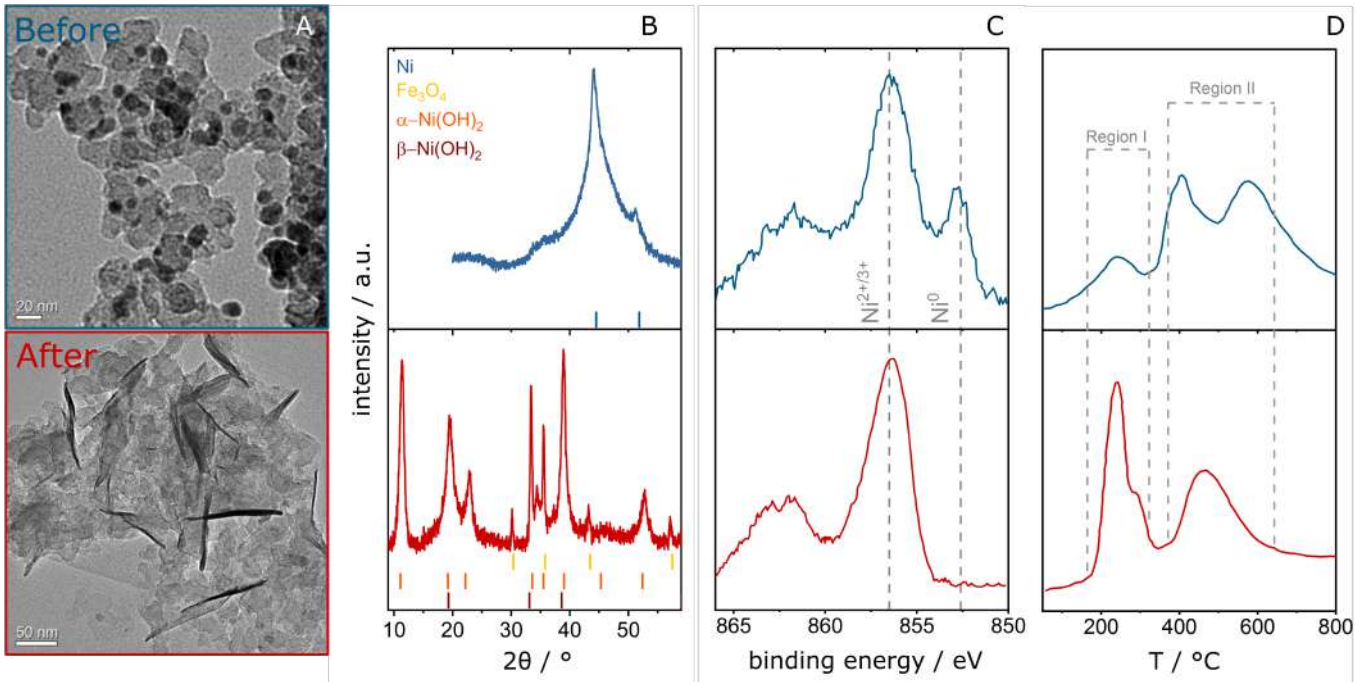


*Figure 3. Physical characterization of $Ni_3Fe$ before and after chemical aging. A) TEM, B) XRD, C) XPS, and D) $H_2$-TPR.*

### 2.1.4 Fuel Cell Testing

After optimization of the catalyst to a ratio of $Ni_7Fe$, we finally tested the two electrocatalysts in an AEMFC setup.[7] A 5 $cm^2$ electrochemical cell was assembled by pressing together a $Ni_7Fe$/C electrocatalyst-coated membrane anode with a N-doped carbon gas diffusion cathode. **Figure 4 a-b** show the experimental setup. **Figure 4c** shows the resulting polarization curve of the cell. This cell shows promising performance with a maximum power density of 56 mW $cm^{-2}$ at a current density of 138 mA $cm^{-2}$. In particular, the cell achieved a limiting current density higher than 200 mA $cm^{-2}$. To the best of our knowledge, this is the highest current density value reported to date and is twice as high as the limiting current densities reported for AEMFCs using PGM-free electrocatalysts in both the anode and the cathode.

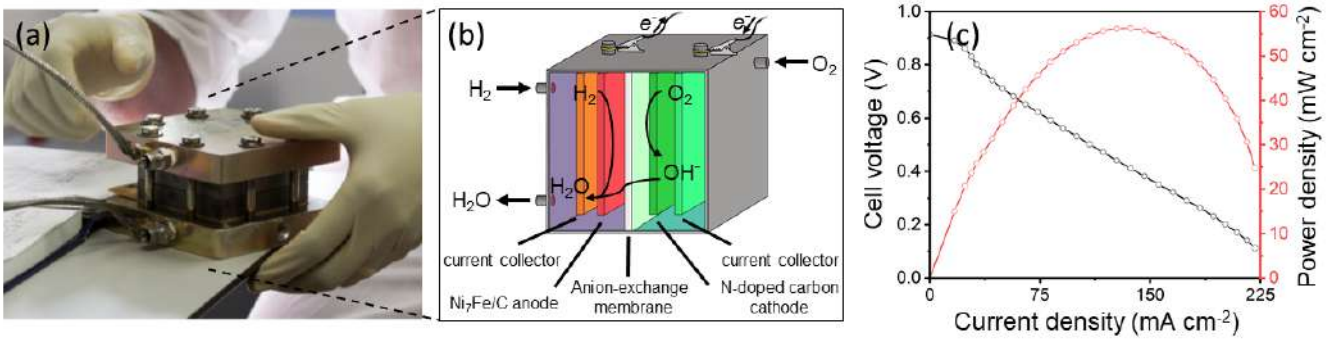


*Figure 4 (a) Photo and (b) schematic of the AEMFC setup. (c) Polarization curve of the AEMFC with $Ni_7Fe$/C anode and N-doped carbon cathode catalysts. $T_{cell}$ = 95 °C, RH 100%, flow rates of 0.01 l pm of $H_2$ (2 bar gauge) and 0.2 lpm of $O_2$ (no back pressure) for anode and cathode, respectively.*

# 3 NICKEL(NITRIDE) SUPPORTED ON NITROGEN-DOPED CARBON AND ITS DOPING WITH ULTRALOW PT CONTENT

## 3.1.1 SYNTHESIS AND CHARACTERISATION (CNRS)

An additional explorative effort was carried out, targeting Ni-nitride materials supported on Ketjenblack 600 JD. Indeed, recent reports highlight the potential of such materials[8] for the HOR, exhibiting activity nearing those of Pt up to 0.26 V vs. RHE in 0.1 M KOH. Here, we synthesized several Ni electrocatalysts supported on carbon using a wet impregnation followed by one, or several pyrolysis, aiming to first synthesize metallic Ni nanoparticles supported on carbon and, then, insert nitrogen in the catalyst crystalline structure to form $Ni_xN$/C. Specifically, two syntheses were performed by mixing Ketjenblack with $NiN_2O_66H_2O$ in MilliQ water (18.2 MΩ) and also optionally with urea (the latter being known for its reductive capabilities during pyrolysis). The 2 or 3 precursors were stirred for 24 h, followed by a drying step overnight at 85°C and a ball-milling at 200 rpm for 1 h. The electrocatalyst precursors were then pyrolyzed under 5% $H_2$ at 550°C for 1 h, aiming at a 50 wt. % Ni loading on the carbon support. The samples are labelled Ni/KJB and Ni/KJB-urea. The XRD showed that metallic Ni nanoparticles were obtained, (**Figure 5a**). The overall crystallite size decreased from 10 nm in Ni/KJB to 8 nm in Ni/KJB-urea. The effect of an additional heat treatment in $NH_3$ at 350°C for 3h was investigated, aiming to obtain $Ni_xN$. However, this treatment resulted in no formation of $Ni_xN$. Thus, other pyrolysis parameters were explored. A mixture of $Ni_xN$, Ni(0) and $NiO_x$ was obtained by directly heat treating the nickel precursor and the carbon support at 275°C, with flash pyrolysis and/or heating ramp conditions, as presented in **Figure 5b.** Finally, the effect of the decoration of Ni/KJB with 2 wt. % Pt was investigated. The Pt nanoparticles were synthesized by a polyol-assisted method. The colloidal solution was collected and a calculated amount was added to Ni/KJB dispersed in a 5:1 mix of $H_2O$:EtOH. The solution was stirred in an ultrasonic bath overnight, before filtration and drying at 85°C.

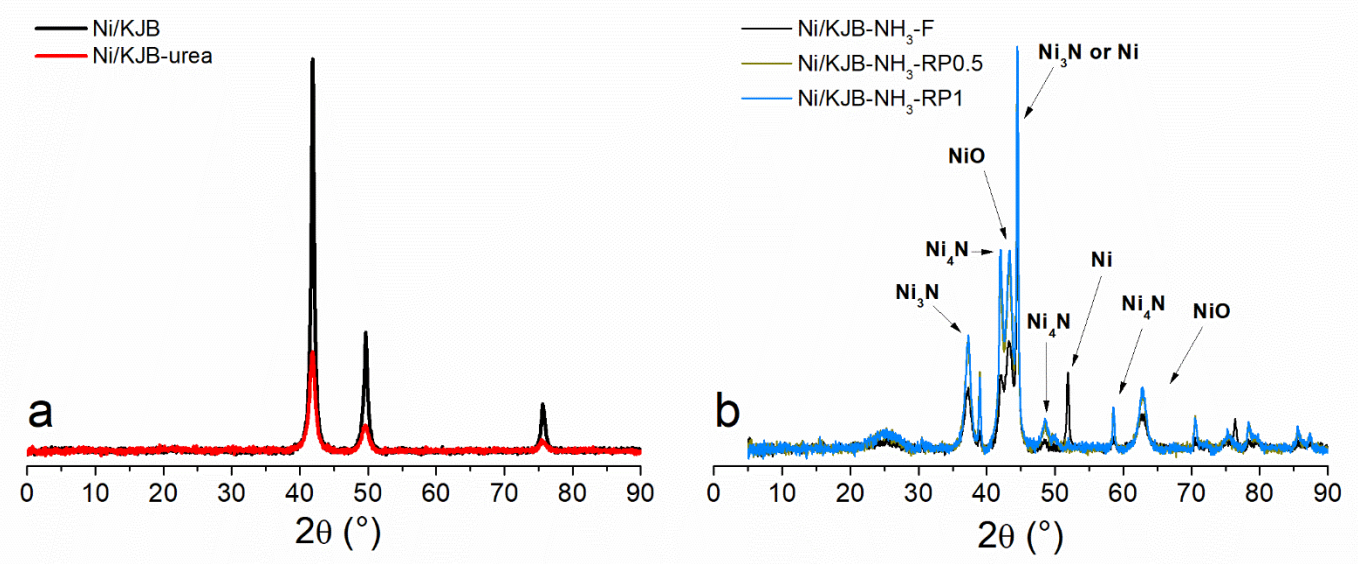


*Figure 5 XRD patterns of (a) Ni/Ketjenblack (KJB) and Ni/KJB-urea and (b) a second set of materials derived from Ni/KJB by applying different temperature-time trajectories during the second heating in ammonia (namely, flash pyrolysis with a 1h dwelling time at 275°C, or ramping to 275°C at a ramp rate of 0.5 or 1°C/min, without any dwelling at 275°C).*

### 3.1.2 Electrochemical Activity in Liquid Electrolyte

Despite differences in nanoparticle size, the Ni/KJB and Ni/KJB-urea electrocatalysts exhibit similar HOR activity in $H_2$-saturated 0.1 M KOH (1600 rpm, 5 mV $s^{-1}$), as presented in **Figure 6a**. The electrocatalysts exhibit an HOR onset near 0 V vs. RHE and HOR current density up to 0.5 – 0.7 mA $cm^{-2}_{geo}$ (difference between the curves measured in $H_2$- and $N_2$-saturated electrolytes) which is maintained up to ca. 0.25 V vs. RHE, prior to surface deactivation (**Figure 6a**). Surprisingly, the Ni/KJB-$NH_3$ electrocatalysts whose XRD patterns are reported on **Figure 5b** presented no catalytic performance for the HOR. Last, the addition of 2 wt. % of Pt on Ni/KJB (labelled Pt/Ni/KJB) resulted in a substantial increase in activity in 0.1 M KOH, as evidenced by the $j_{H2} – j_{N2}$ current densities presented in **Figure 6b**, where this material reaches a current density at 0.05 V vs. RHE of 1.07 mA $cm^{-2}_{geo}$, vs. only 0.42 mA $cm^{-2}_{geo}$ for Ni/KJB and ca. 2.1 mA $cm^{-2}_{geo}$ for 40 wt. % Pt and PtRu/C. Additionally, the electrocatalyst is able to maintain its activity at potentials > 0.25 V vs. RHE, thus indicating that the platinum is likely helping in maintaining the nickel activity beyond its usual deactivation potential, likely by reducing the surface nickel oxides. After correction for diffusion limitation by the Koutecky-Levich analysis, the kinetic current density at 0.05 V vs RHE of Pt/Ni/KJB is estimated to be 1.87 mA $cm^{-2}$, close to the internal project target of 2.2 mA $cm^{-2}$ set for CRM-free catalyst.

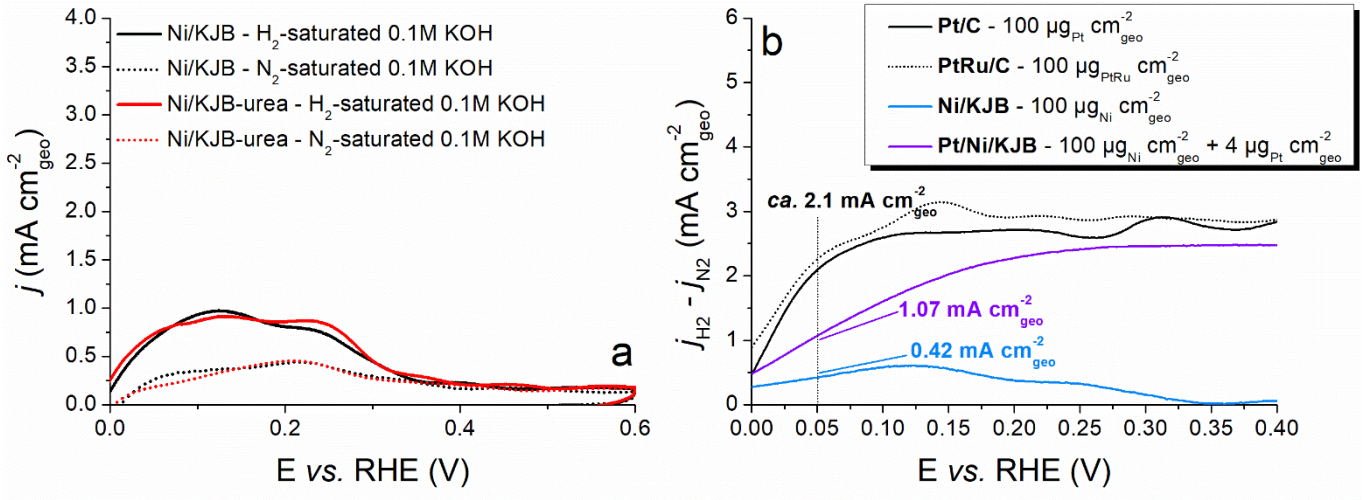


***Figure 6.*** *Cyclic voltammetry in 0.1 M KOH for (a) Ni/KJB and Ni/KJB-urea measured In $N_2$ or $H_2$ saturated electrolyte; (b) for commercial 40 wt. % Pt/C, 40 wt% PtRu/C, and laboratory Ni/KJB (50 wt% Ni) and 2 wt. % Pt on Ni/KJB in $H_2$ saturated electrolyte (data corrected for the current measured in $N_2$ saturated electrolyte). The experimental conditions for the electrochemistry were 5 mV/s, 1600 rpm, $N_2$ or $H_2$-saturated 0.1 M KOH. The Nickel loading was 100 µg $cm^{-2}_{Nickel}$.*

### 3.1.3 Fuel Cell Testing

The Pt/Ni/KJB sample was subsequently tested as an anode in AEMFC, paired with a Fe-N-C electrocatalyst (0.85 mg $cm^{-2}$) at the cathode. The anode loading was 0.95 $mg_{Ni}$ $cm^{-2}_{geo}$ and 0.038 $mg_{Pt}$ $cm^{-2}_{geo}$. A carbon/ionomer (Fumasep®) ratio of 0.4 was chosen for the anode catalytic layer. A Fumapem® (10 µm thickness) was used to separate the two electrodes. The electrocatalyst was characterized at 60°C, leading to the performances presented in **Figure 7** and a peak power density of 90 mW $cm^{-2}$. The performances remains far lower than for state-of-the-art 40 wt. % PtRu/C at the anode, *i.e.* 540 mW $cm^{-2}$, but are not as low as one could expect if normalized by the anode PGM loading (40 vs 400 µg PGM/$cm^2$ at anode, i.e. a factor 10). As revealed also by RDE data, this indicates a possible synergy between Ni sites and Pt sites for the HOR. The location and relative contents of Pt and Ni in the catalyst, the catalyst loading, and its implementation in MEA however still require optimization.

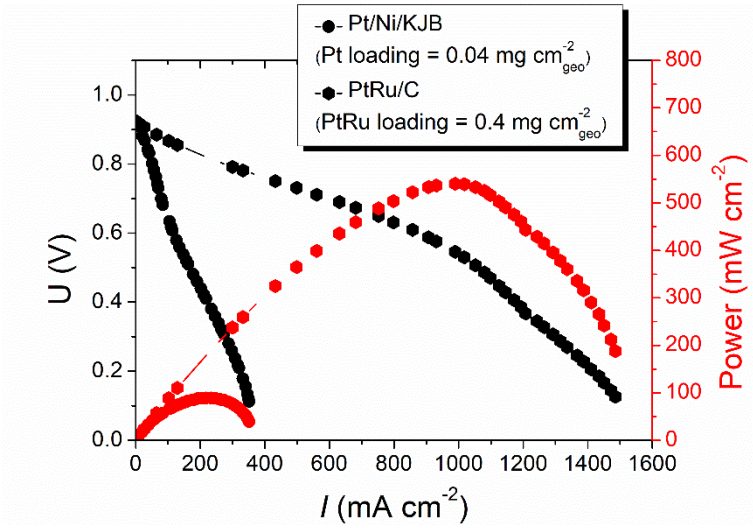


*Figure 7. AEMFC performance with i) Pt/Ni/KJB anode and $Fe_{0.5}$-$NH_3$ cathode and (ii) 40 wt. % PtRu/C anode and $Fe_{0.5}$-$NH_3$ cathode. The performances were measured at 60°C. 1 bar of backpressure were applied at both the anode and the cathode.*

### 3.2 CONCLUSIONS AND COMPARISON TO INTERNAL CREATE TARGETS

Since they are immune to dissolution in alkaline electrolyte at typical potentials experienced during HOR (0-0.2 $V_{RHE}$), Ni, Co and Fe based HOR metallic catalysts are promising as PGM-free base metals. However, their thermodynamic limit of oxidation at potentials of only *ca* 0.2 $V_{RHE}$ requires optimization in half cell potential limits at the anode. Especially $O_2$ infiltration upon start/stop events needs to be avoided to keep anode potentials below the thermodynamic limit of Ni oxidation.

While none of the developped PGM-free (CRM-free) HOR catalysts reached the internal CREATE activity target defined for the RDE setup (2.2 mA $cm^{-2}$ of kinetic current density at 0.05 $V_{RHE}$ and for a loading of 200 µg $cm^{-2}$), promising advance toward the internal target (1.07 mA $cm^{-2}_{geom}$ and 1.87 mA $cm^{-2}$ after correction for diffusion limitation, at 0.05 V vs RHE) was achieved by functionalizing a Ni/C catalyst with 2wt% Pt.

In AEMFC, we have built a completely PGM and CRM-free AEMFC using $Ni_7Fe$/C and N-doped carbon electrocatalysts at the anode and cathode, respectively. The cell achieved a maximum power density of 56 mW $cm^{-2}$ at a current density of 138 mA $cm^{-2}$, which is among the highest value reported to date for CRM-free electrocatalyst systems. Another MEA with a Fe-N-C cathode and 2%Pt/Ni/C (40 $\mu g_{Pt}$ $cm^{-2}$) achieved a maximum power density of 87 mW $cm^{-2}$ at circa 200 mA $cm^{-2}$. The cells with no or low PGM at the anode have high onset potentials (comparable to those with high PtRu anode contents) and good cell performance at low current density (< 10 mA $cm^{-2}$) but fail to achieve high current density. Comparison of the RDE and AEMFC results also show that it is difficult to predict anode performance solely from RDE HOR results, as shown by the promising HOR RDE activity of Pt/Ni/KJB, but hitherto modest cell performance. Novel anode design and understanding of the phenomena controlling an anode operating at high current density will be needed to improve the performance of PGM-free and/or ultralow PGM anodes.

# 4 HER CATALYST

## 4.1 NiMo ALLOYS

### 4.1.1 SYNTHESIS OF NiMo MODEL CATALYSTS (JUELICH)

NiMo alloys are reportedly of interest for HER.[9] Model NiMo alloy catalysts of a 2D geometry were synthesized by arc melting of the pure elements (99.9%, Goodfellow) in Ar atmosphere. The process was repeated eight times to achieve homogeneous alloying of the compositions (1:0, 6:1, 4:1, 3:1, 2:1, 1:1, 0:1). Samples were then cut, embedded in graphite composite, and polished using $AlO_x$ slurry (0.05 µm, Struers) on a polishing pad (MD Mol, Struers).

### 4.1.2 ELECTROCHEMICAL ACTIVITY AND STABILITY (JUELICH)

Potential dependent dissolution was measured online using a NexION 350X ICP-MS (Perkin Elmer) connected to a custom build electrochemical scanning flow cell (SFC). To investigate the impact of Mo on the HER activity of Ni, a set of bulk cell electrochemical measurements were conducted in a custom made PEEK cell, that held the samples. A modified RDE tip was used merely for stirring the solution at 500 rpm. LSV were then obtained in 1 M NaOH (99.99%, Merck Suprapur®) from 0.1 – −0.4 $V_{RHE}$ before and after an AST.

### 4.1.3 ELECTROCHEMICAL ACTIVITY AND STABILITY RESULTS

To understand the impact of alloying Ni for HER applications, we used uniform 2D alloy crystals to exclude effects altering surface area and support porosity. We present online dissolution of various NiMo alloy crystallites in **Figure 8**. Previously, XRD has shown consistent alloying behavior.[9] Due to the thermodynamic limits of $Mo^0$, we observe severe corrosion upon oxidation to a dissolved species.[10] This corrosion can be suppressed at HER potentials during which Mo stays reduced, but the simulated start/stop events and OCV measurements show a consistent trend. The more Mo is present in the alloy, the more of it leaches from the electrode surface. Therefore, the more leaching occurs, the more electrode roughening should occur. Since Ni is immune to dissolution a Ni-rich surface, with varying porosity depending on initial Mo content, remains. The influence of such a roughening alters the electrochemical activity towards HER.

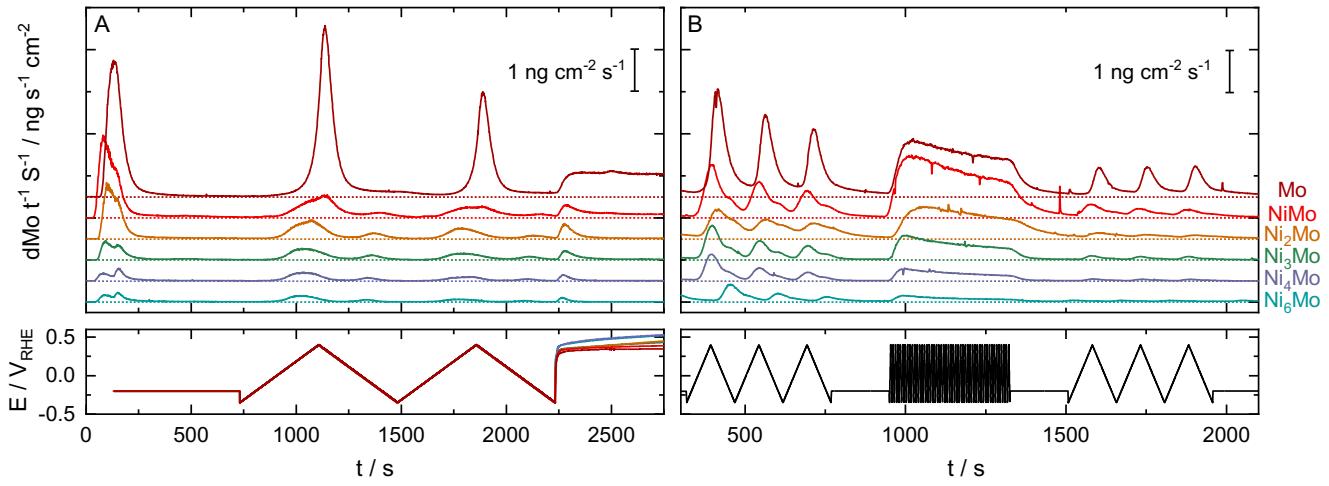


*Figure 8. Mo dissolution rates of different NiMo alloys during potential cycling from HER conditions to OCV to imitate start/stop conditions.*

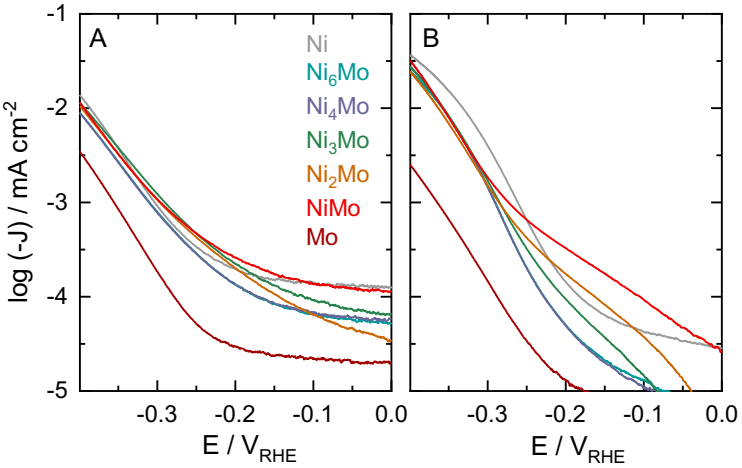


*Figure 9. Activity of NiMo alloys and the pure metals before (A) and after (B) 350 CVs from -0.1 to 0.4 $V_{RHE}$.*

**Figure 9A** shows the HER activity of all alloys right after immersing them in 0.1 M KOH. Only at small current densities, a difference in capacitive currents is observed, while the HER region is identical. This suggests that alloying has no electronic or synergistic effect on Ni. Merely after an AST, where a lot of Mo has dissolved, leaving various surface roughness, a trend in activity can be seen. Here the highest Mo content shows the lowest HER overpotentials, which increases with decreasing initial Mo content and, therefore surface area.

#### 4.1.4 Conclusions

Ni remains a material of interest for HER, however, alloy materials such as Mo can only be used as a sacrificial component which needs to be leached before use in a catalyst layer. Similar to Raney-Ni it can improve the surface area of Ni.

### 4.2 Heteroatom Doped Carbons

#### 4.2.1 Synthesis of Heteroatom Doped Carbons (Technion)

Hetero-doped carbons were synthesized by planetary ball milling of graphite in the presence of heteroatom precursor (four different precursors, leading to four samples). First, the stainless-steel jar (80 ml) was loaded with ~125 g of stainless-steel balls (diameter 5 mm, weight 0.5 g), graphite, and heteroatom precursors and fixed in the ball-milling setup. Then the jar was charged and discharged with ten cycles of argon with a cylinder pressure of one bar to remove the air from the capsule. The mixture was then ball milled at 500 rpm for 16 consecutive cycles of 30 min with 10 min cool-down period. The mixture was exposed to air to terminate the residual carbon free radical. Then the product was collected from the jar and Soxhlet extracted in organic solvents to remove heteroatoms impurities. After the initial cleaning, the catalysts were washed twice with 5% HCl to remove any metal impurities and dried in a vacuum oven for 10 h at 60°C. The four different heteroatom-doped carbons were labelled as sample 1, 2, 3 and 4.

#### 4.2.2 Electrochemical Activity and Stability (Aalto)

To evaluate the ability of the heteroatom doped carbons to promote the HER, the electrochemical HER activity was investigated in an RDE setup, following by the stability test AST No. 4 (5,000 LSV between 0 and 0.4 V vs. RHE, at 100 mV/s, in $N_2$-satd electrolyte) in accordance to CREATE Deliverable 2.1. Four samples, based on a different heteroatom doped carbon, were tested in a three-electrode setup using glassy carbon (GC) as a working, an Ir-wire in an external compartment as a counter and RHE as a reference

electrode. **Figure 10a and 10b** show the HER polarization curves of *Sample 1, 2, 3* & *4* measured before and after AST4, respectively. Commercially available Pt (20 w%) on carbon was measured as reference material.

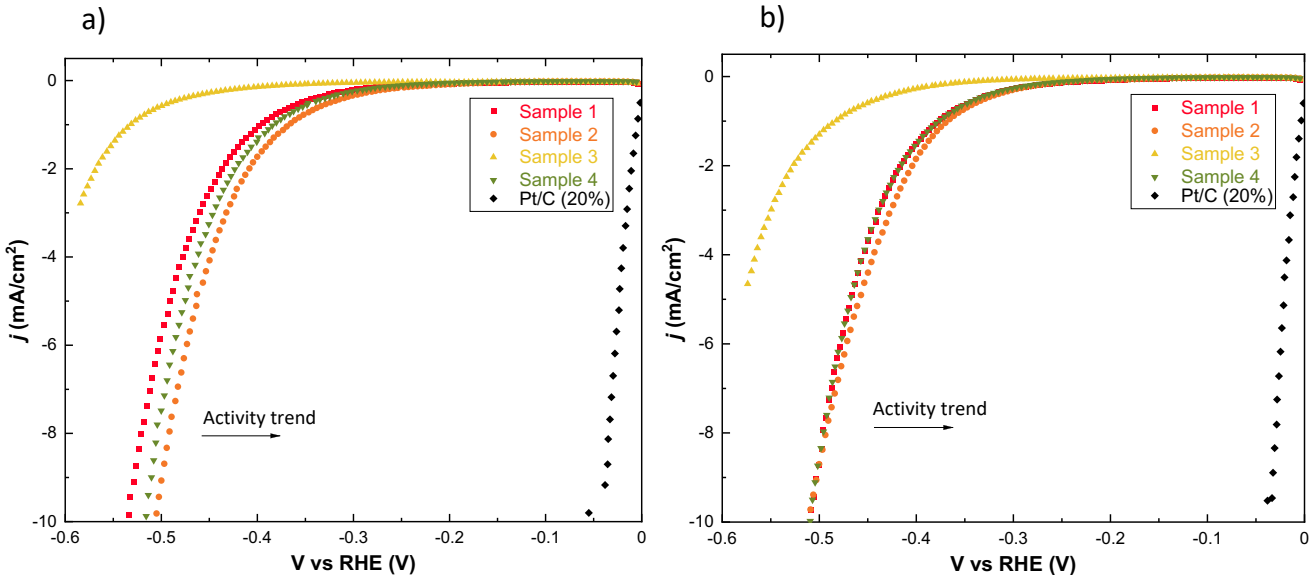


***Figure 10.*** *HER polarization curves of heteroatom doped carbons a) before AST4 test, b) after AST4 test, compared with Pt 20% on C. Scan rate 2 mV/s, rotation speed 2500 rpm, $H_2$ saturated 0.1 M KOH. Catalyst loading 0.2 mg cm$^{-2}$, normalized with geometric surface area.*

From the HER polarization curves, *Sample 2* has the highest activity and stability before and after AST4 among the heteroatom doped carbon samples. In case of *Samples 1* and *4*, the activities are similar to each other before but overlapped after the AST4. A plausible reason is the availability of more electrochemical surface area after the AST4 due to surface wetting. A similar trend is observed for *Sample 3* where the activity trend shifted towards low overpotential region after the AST4. All samples except *Sample 3* have outperformed the CRM-free N-MWCNT[11] with onset potential of 300 mV vs RHE compared to 370 mV vs RHE in the low overpotential region. However, $\eta_{HER,10}$ = 500 mV of *Sample 2* is higher than $\eta_{HER,10}$ = 370 mV of N-MWNT.

### 4.2.3 Conclusions and comparisons to internal CREATE Targets

The electrochemical analysis of heteroatom doped carbon materials has shown a promising performance towards HER in alkaline medium in comparison to the ones reported in the literature. However, they do not meet the pass criteria for initial catalyst activity set in Deliverable 2.1 (namely, ≥ 2.2 mA cm$^{-2}$ at -0.5 $V_{RHE}$) and hence, have not been selected for electrolyzer investigations.

## 4.3 Ni and Fe on CNTs

### 4.3.1 Synthesis of NiFe based Catalysts (Aalto)

The catalysts were synthesized with ALD method and further annealing process. Ni/CNTs and Fe/CNTs were obtained by depositing Ni or Fe precursors onto CNTs, and NiFe/CNTs was obtained by codepositing Ni and Fe on CNTs in one batch, with ALD. All of these catalysts were annealed at high temperatures after ALD.

Due to the low sublimation temperature of the ALD precursors, the metal loading after annealing (**Table 1**) is less than the loading resulted from ALD (**Table 2**). The EDS data in **Table 2** show that the metal content increased obviously from CNTs to Ni/CNTs or NiFe/CNTs.

*Table.1 Mass change after ALD reaction.*

| | Mass before reaction /g | Mass after reaction /g | Difference | Percentage increased |
|---|---|---|---|---|
| Fe/CNTs | 0.0651 | 0.0919 | 0.0268 | 41.17% |
| Ni/CNTs | 0.1029 | 0.1267 | 0.0238 | 23.13% |
| NiFe/CNTs | 0.0997 | 0.1174 | 0.0177 | 17.75% |

*Table.2 EDS of metal content of CNTs, Ni/CNTs and NiFe/CNTs.*

| CNT+Nafion | | | NiFe/CNT+Nafion | | | Ni/CNT+Nafion | | |
|---|---|---|---|---|---|---|---|---|
| Element Line | Norm. Wt.% | Atom % | Element Line | Norm. Wt.% | Atom % | Element Line | Norm. Wt.% | Atom % |
| C K | 63.95 | 74.59 | C K | 72.87 | 84.8 | C K | 76.06 | 87.4 |
| O K | 2.31 | 2.02 | O K | 0 | 0 | O K | 0 | 0 |
| F K | 30.52 | 22.51 | F K | 17.17 | 12.63 | F K | 13.2 | 9.59 |
| Na K | 0 | 0 | Na K | 0 | 0 | Na K | 0.94 | 0.56 |
| S K | 0.57 | 0.25 | S K | 0.98 | 0.43 | S K | 0.72 | 0.31 |
| Fe,Ni L | 2.65 | 0.63 | Fe,Ni L | 8.98 | 2.14 | Fe,Ni L | 9.08 | 2.14 |
| Total | 100 | 100 | Total | 100 | 100 | Total | 100 | 100 |
| C from Nafion | 9.65 | 11.26 | C from Nafion | 5.43 | 6.32 | C from Nafion | 4.17 | 4.80 |
| C from CNTs | 54.30 | 63.34 | C from CNTs | 67.44 | 78.49 | C from CNTs | 71.89 | 82.61 |
| Fe,Ni/CNTs | 4.88 | 0.63 | Fe,Ni/CNTs | 13.31 | 2.14 | Fe,Ni/CNTs | 12.63 | 2.14 |

The low loading of metals could also be reflected in the XRD patterns of the materials, as shown in **Figure 11**. No obvious new Ni or Fe peaks can be observed compared to the original CNTs, which suggest that the loadings of Ni and Fe are quite low or they do form crystalline moieties. The shift of the wide carbon peak at 20~30 degree towards higher value is caused by the annealing process.

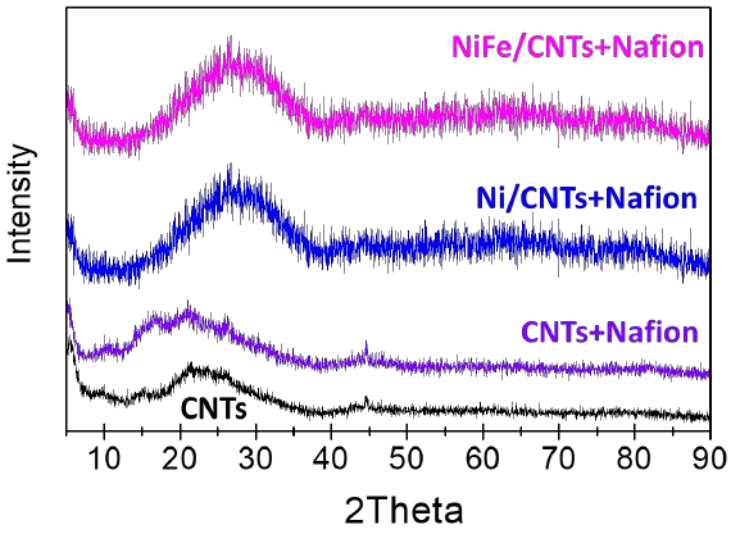


*Figure 11. XRD patterns of the original CNTs, CNTs with Nafion, Ni/CNTs with Nafion and NiFe/CNTs with Nafion.*

With such low metal loading, nanoparticles still could be seen on CNTs in the SEM images as shown in **Figure 12**. Nanoparticles could be seen easily at the surface of Ni/CNTs, while the particles in NiFe/CNTs are not so easy to find under the SEM view. So, the addition of Fe in NiFe/CNTs affects the morphology of the nanoparticles.

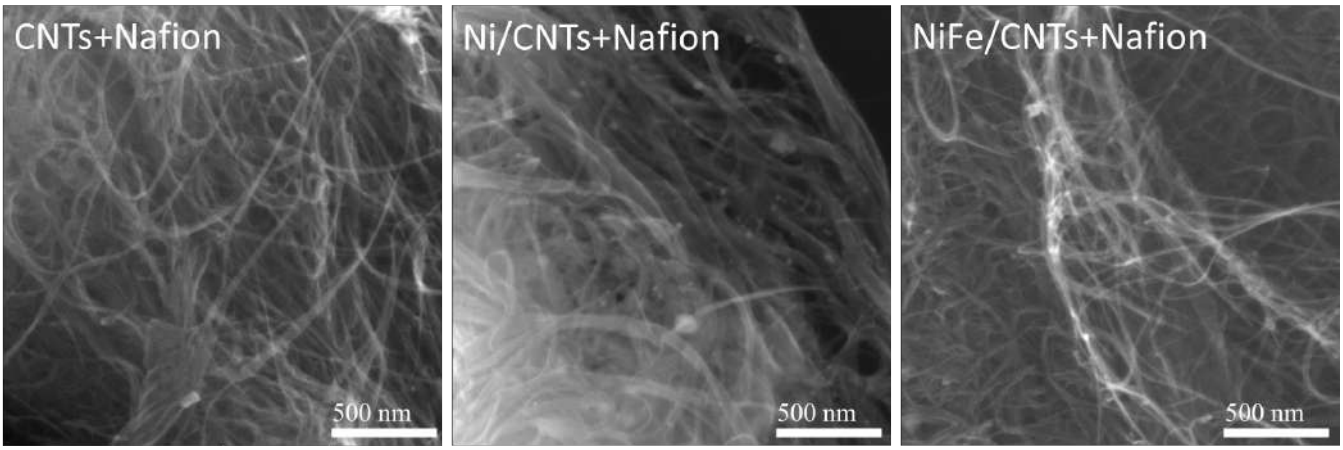


*Figure 12. SEM images of CNTs with Nafion, Ni/CNTs with Nafion and NiFe/CNTs with Nafion.*

### 4.3.2 Electrochemical Activity and Stability (Aalto)

The activity of the Ni and Fe based catalysts were evaluated with an RDE setup in $H_2$ saturated 0.1 M KOH (**Figure 13**), following by the stability test AST-9 (5,000 LSV between 0 and -0.4 V vs RHE in $N_2$ saturated 0.1 M KOH) (**Figure 10**), in accordance to CREATE **Deliverable 2.1**. Three samples, i.e. Fe/CNTs, Ni/CNTs and NiFe/CNTs, were tested in a three-electrode setup using glassy carbon (GC) as a working electrode. A graphite rod and Hg/HgO electrode were used as a counter and reference electrode, respectively. A commercial 20% Pt/C catalyst was measured as a reference material.

Both Ni/CNTs and NiFe/CNTs show better performance than Fe/CNTs as shown in **Figure 13**. This may be caused by the better intrinsic HER activity of Ni in alkaline. NiFe/CNTs shows slightly better performance than Ni/CNTs while HER onset potentials is about -200 mV vs. RHE for both of them. At 10 mA/cm$^2$, the overpotentials needed for Ni/CNTs and NiFe/CNTs are around 400 mV, which are about 300 mV larger than for commercial 20% Pt/C.

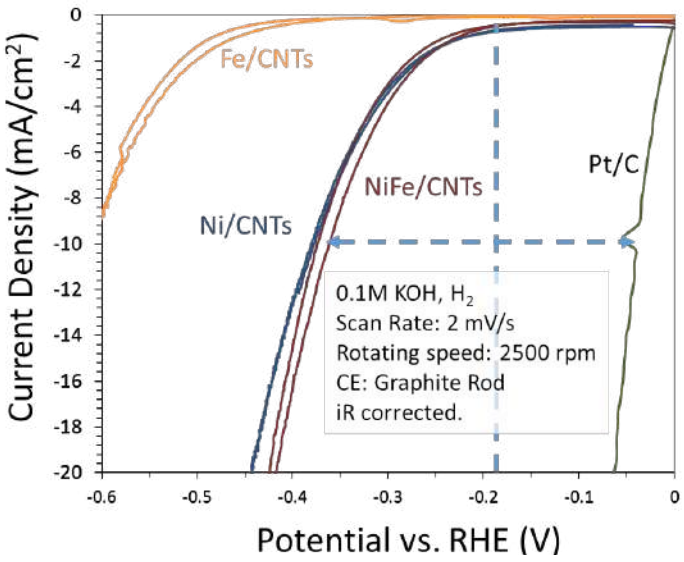


*Figure 13. HER activities of Fe/CNTs, Ni/CNTs and NiFe/CNTs in $H_2$ saturated 0.1M KOH. WE: catalysts on glassy carbon. CE: graphite rod. RE: Hg/HgO. Scan rate 2 mV/s, rotation speed 2500 rpm. Catalyst loading 0.2 mg $cm^{-2}$, normalized with geometric surface area. All the data are iR-corrected and the potentials have been converted to potentials vs. RHE.*

Both Ni/CNTs and NiFe/CNTs show good stability after 5000 cycles' CV test from 0 to -0.4 V vs. RHE, as shown in **Figure 14**. The performance was almost unchanged after the AST9 test. Compared with other catalysts without precious metal in this project, the performance of Ni/CNTs and NiFe/CNTs are comparable.

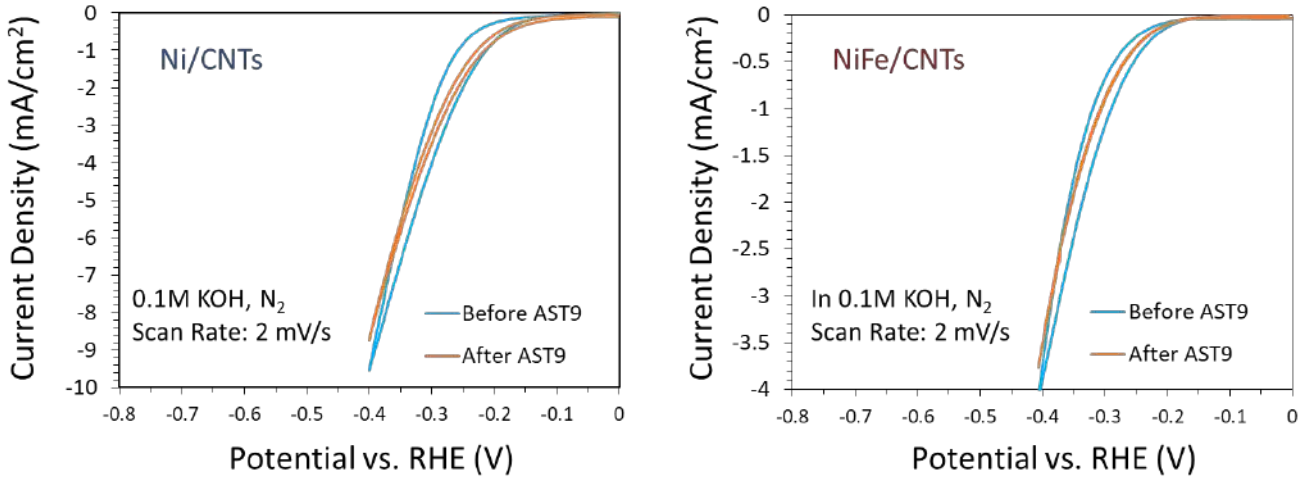


*Figure 14. HER polarization curves before and after AST-9. Scan rate 2 mV/s, rotation speed 800 rpm, $N_2$ saturated 0.1 M KOH. Catalyst loading 0.2 mg $cm^{-2}$, normalized with geometric surface area. All the data are iR corrected and the potentials have been converted to potentials vs. RHE.*

### 4.3.3 Conclusions and comparison to internal CREATE Targets

In conclusion, with ALD method, we obtained two non-precious metal catalysts, i.e. Ni/CNTs and NiFe/CNTs, for HER in 0.1 M KOH with low metal loading and good stability. Applying the targeted loading, non-PGM catalysts in liquid electrolyte did not pass the internal stage-gate of HER activity (≥ 200 mV below the targeted potential at 2.1 mA $cm^{-2}$).

# 5 REFERENCES

1. Davydova, E. S.; Speck, F. D.; Paul, M. T. Y.; Dekel, D. R.; Cherevko, S., Stability Limits of Ni-Based Hydrogen Oxidation Electrocatalysts for Anion Exchange Membrane Fuel Cells. *ACS Catal.* **2019**, 6837-6845.
2. Davydova, E.; Zaffran, J.; Dhaka, K.; Toroker, M.; Dekel, D., Hydrogen Oxidation on Ni-Based Electrocatalysts: The Effect of Metal Doping. *Catalysts* **2018,** *8* (10).
3. Brito, J. L.; Laine, J., Reducibility of Ni-Mo/Al2O3 Catalysts: A TPR Study. *J. Catal.* **1993,** *139* (2), 540-550.
4. Scheffer, B.; Molhoek, P.; Moulijn, J. A., Temperature-programmed reduction of NiOWO3/Al2O3 Hydrodesulphurization catalysts. *Appl. Catal.* **1989,** *46* (1), 11-30.
5. Dongil, A. B.; Ghampson, I. T.; García, R.; Fierro, J. L. G.; Escalona, N., Hydrodeoxygenation of guaiacol over Ni/carbon catalysts: effect of the support and Ni loading. *RSC Adv.* **2016,** *6* (4), 2611-2623.
6. Speck, F. D. Degradation Mechanisms of Electrocatalysts in Alkaline Media. 2020.
7. Biemolt, J.; Douglin, J. C.; Singh, R. K.; Davydova, E. S.; Yan, N.; Rothenberg, G.; Dekel, D. R., An Anion-Exchange Membrane Fuel Cell Containing Only Abundant and Affordable Materials *Submitted, under Review* **2020**.
8. Ni, W.; Krammer, A.; Hsu, C. S.; Chen, H. M.; Schuler, A.; Hu, X., Ni3 N as an Active Hydrogen Oxidation Reaction Catalyst in Alkaline Medium. *Angew Chem Int Ed Engl* **2019,** *58* (22), 7445-7449.
9. Schalenbach, M.; Speck, F. D.; Ledendecker, M.; Kasian, O.; Goehl, D.; Mingers, A. M.; Breitbach, B.; Springer, H.; Cherevko, S.; Mayrhofer, K. J. J., Nickel-molybdenum alloy catalysts for the hydrogen evolution reaction: Activity and stability revised. *Electrochim. Acta* **2017**.
10. Pourbaix, M., *Atlas of Electrochemical Equilibria in Aqueous Solutions*. NACE International: 1974.
11. Davodi, F.; Tavakkoli, M.; Lahtinen, J.; Kallio, T., Straightforward synthesis of nitrogen-doped carbon nanotubes as highly active bifunctional electrocatalysts for full water splitting. *Journal of Catalysis* **2017,** *353*, 19-27.